A00-39806

AIAA Paper 2000-4421

CONTROL OF HOVERING SPACECRAFT USING ALTIMETRY *

S. Sawai† and D.J. Scheeres‡
Department of Aerospace Engineering
The University of Michigan
Ann Arbor, MI 48109-2140

June 13, 2000

Abstract

The control of a spacecraft hovering over a uniformly rotating asteroid is analyzed. This work builds on the previous analysis of open-loop stability of hovering spacecraft trajectories (Scheeres 1999) by considering the effect of closed-loop control strategies on the overall stability of the hovering trajectory. We characterize the ability of one-dimensional altimetry measurements to stabilize the hovering spacecraft and find some ideal control methodologies that can yield stable hovering trajectories. These ideas are developed initially for the ideal case of a spherical asteroid and are then applied to a rotating ellipsoid and a rotating model of the asteroid Castalia (Hudson and Ostro 1994). The necessary modifications to the measurement and control laws in these more general gravitational cases are characterized.

Introduction

Performing scientific explorations of small bodies such as comets and asteroids can be simplified in many cases by abandoning an "orbital" approach (Scheeres et al. 2000) in favor of a "hovering" approach (Scheeres 1999) where the spacecraft thrusts continuously (or near-continuously) to null out the gravitational and rotational accelerations that act on it, fixing its position in the body fixed frame. Such an approach to exploration would make it possible to obtain high resolution measurements, and even samples, from multiple sites over the body surface without having to make complicated transitions from orbital to body-fixed trajectories between each near-surface observation period. The implementation of such hovering trajectories are not trivial, however, as they are fundamentally unstable (Scheeres 1999) and may involve the complex interplay of several navigation sensors and control actuators to implement.

In this paper we investigate the feasibility of simplifying the navigation of these hovering trajectories by applying a simple control law that stabilizes the hovering trajectory. If the hovering trajectory can be stabilized with a simple closed control loop, the complexity of the entire navigation problem can be similarly reduced. Ideally, the stabilizing control loop can then run in the "background" and a more sophisticated control loop can be used to "drive" the hovering spacecraft over the small body surface. Ideally, these higher-level control laws will be simpler to implement and characterize if the underlying stability of the hovering trajectory is ensured.

Our proposed approach to stabilizing the hovering trajectory uses a single altimeter and thrusting direction. By tightly controlling the spacecraft altitude along the direction that the small body gravity acts, we show that it is possible to completely stabilize the hovering trajectory in most cases of interest. We define and analyze the stability and implementation of this control for a spacecraft hovering over a rotating sphere, ellipsoid, and a generalized shape based on the asteroid Castalia (Hudson and Ostro 1994). We note that our control law does not uniformly stabilize a hovering trajectory, but is only valid for hovering less than a characteristic "altitude", defined in the text. We present some limited simulations of the approach to verify its utility.

†Visiting Scholar; and also Research Associate, Institute of Space and Astronautical Science, Japan; email: sawai@newslan.isas.ac.jp

‡Assistant Professor of Aerospace Engineering; Senior Member AIAA; email: scheeres@umich.edu

Consideration of Controller Type

The previous work of (Scheeres 1999) assumed open-loop control to cancel out the centrifugal force and gravity attraction. Control thrusts are added as a quasi-continuous constant acceleration which balances the residual acceleration if the spacecraft is at the prescribed hovering point. In this paper, we assume a closed-loop controller in addition to the open-loop one. The easiest way to control the spacecraft is to keep the altimetry output constant. So, this paper considers such "tight" controllers. With such a simple control logic, hovering can be easily implemented.

For the control direction, the nominal direction of the gravitational acceleration meets at the prescribed point is adopted. With the tight control using the gravity direction for observation and thrusting, we do not have to install open-loop continuous thrusting to kill out the nominal gravity attraction. It can be canceled through the closed-loop tight control. In general, it is difficult to estimate the magnitude of gravity attraction exactly. If the open-loop gravity is specified, it may cause the hovering point to be disturbed due to error.

Stability of Controller

For now, it is assumed that the nominal gravity force and centrifugal force are canceled by open-loop continuous thrusting. This means that the nominal prescribed position is an equilibrium point for hovering. But from (Scheeres 1999) we see that equilibrium points of hovering are not stable for most positions without closed-loop control. In this section, we discuss the stability of hovering with the linearized equation of motion, and investigate how the stability can be enhanced by adding a "tight" closed-loop control along the nominal gravity direction. At first, we consider the case when the center body is a point mass, followed by the consideration of an arbitrarily shaped body.

Stability Analysis of Point Mass Center Body In this case, stability around the equilibrium point can be investigated analytically. By taking the coordinate of Fig.1, the equation of motion becomes

$$\ddot{\mathbf{r}} + 2\omega\mathbf{z} \times \dot{\mathbf{r}} + \omega^2\mathbf{z} \times (\mathbf{z} \times \mathbf{r}) = \mathbf{F}_c + \mathbf{F}_g \quad (1)$$

where

$\mathbf{r} \equiv [x, y, z]^T$

$\mathbf{z} \equiv [0, 0, 1]^T$

ω : Angular velocity of center body

$\mathbf{F}_c$: Control force

$\mathbf{F}_g$: Gravitational force

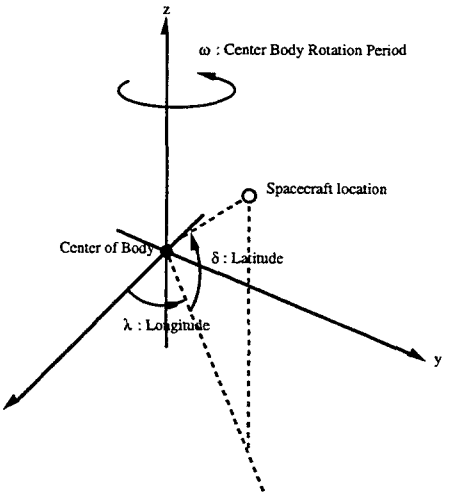

Figure 1: Body fixed Frame Coordinate

By treating the perturbation around the nominal point of $\mathbf{r}_0 = \begin{bmatrix} x_0 \\ 0 \\ z_0 \end{bmatrix}$, the gravity attraction is linearized as

$$\mathbf{F}_g = \left.\frac{\partial U}{\partial \mathbf{r}}\right|_0 + \left[\left.\frac{\partial^2 U}{\partial \mathbf{r}^2}\right|_0\right](\mathbf{r} - \mathbf{r}_0) \quad (2)$$

where $U = \frac{\mu}{r}$

Now, let the coordinates be normalized by the resonance radius of $r_s \equiv \left(\frac{\mu}{\omega^2}\right)^{1/3}$, or

$$r_n \equiv \frac{\|\mathbf{r}_0\|}{r_s} \quad (3)$$

$$x_n \equiv \frac{x_0}{r_s} \quad (4)$$

$$z_n \equiv \frac{z_0}{r_s} \quad (5)$$

$$\Delta x \equiv \frac{x - x_0}{r_s} \quad (6)$$

$$\Delta y \equiv \frac{y}{r_s} \quad (7)$$

$$\Delta z \equiv \frac{z - z_0}{r_s} \quad (8)$$

$$\mathbf{f}_{c,0} \equiv \mathbf{f}_c / r_s \quad (9)$$

and Eq.1 can be linearized as

$$\begin{bmatrix} \Delta\ddot{x} \\ \Delta\ddot{y} \\ \Delta\ddot{z} \end{bmatrix} - \begin{bmatrix} 0 & 2\omega & 0 \\ -2\omega & 0 & 0 \\ 0 & 0 & 0 \end{bmatrix} \begin{bmatrix} \Delta\dot{x} \\ \Delta\dot{y} \\ \Delta\dot{z} \end{bmatrix} - [a_{ij}] \begin{bmatrix} \Delta x \\ \Delta y \\ \Delta z \end{bmatrix} = \mathbf{f}_{c,0} \quad (10)$$

where

$$[a_{ij}] = \begin{bmatrix} \omega^2 & 0 & 0 \\ 0 & \omega^2 & 0 \\ 0 & 0 & 0 \end{bmatrix} + \left[\frac{\partial^2 U}{\partial \mathbf{r}^2} \Big|_0 \right]$$

$$\left[\frac{\partial^2 U}{\partial \mathbf{r}^2} \Big|_0 \right] = \omega^2 \begin{bmatrix} 1 - \frac{1}{r_n^3} + \frac{3x_n^2}{r_n^5} & 0 & \frac{3x_n z_n}{r_n^5} \\ 0 & 1 - \frac{1}{r_n^3} & 0 \\ \frac{3x_n z_n}{r_n^5} & 0 & -\frac{1}{r_n^3} + \frac{3z_n^2}{r_n^5} \end{bmatrix}$$

Using the coordinate of $(\Delta r, \Delta y, \Delta t)$ as fig.2 , or

$$\begin{bmatrix} \Delta r \\ \Delta y \\ \Delta t \end{bmatrix} \equiv \begin{bmatrix} \frac{x_n}{r_n} & 0 & \frac{z_n}{r_n} \\ 0 & 1 & 0 \\ -\frac{z_n}{r_n} & 0 & \frac{x_n}{r_n} \end{bmatrix} \begin{bmatrix} \Delta x \\ \Delta y \\ \Delta z \end{bmatrix} \tag{11}$$

Eq.10 is transformed as follows;

$$\begin{bmatrix} \Delta \ddot{r} \\ \Delta \ddot{y} \\ \Delta \ddot{t} \end{bmatrix} - \frac{2\omega}{r_n} \begin{bmatrix} 0 & x_n & 0 \\ -x_n & 0 & z_n \\ 0 & -z_n & 0 \end{bmatrix} \begin{bmatrix} \Delta \dot{r} \\ \Delta \dot{y} \\ \Delta \dot{t} \end{bmatrix}$$

$$-\frac{\omega^2}{r_n^2} \begin{bmatrix} x_n^2 + \frac{2}{r_n} & 0 & -x_n z_n \\ 0 & r_n^2 - \frac{1}{r_n} & 0 \\ -x_n z_n & 0 & z_n^2 - \frac{1}{r_n} \end{bmatrix} \begin{bmatrix} \Delta r \\ \Delta y \\ \Delta t \end{bmatrix}$$

$$= \begin{bmatrix} f_r \\ f_y \\ f_t \end{bmatrix} \tag{12}$$

where $\begin{bmatrix} f_r \\ f_y \\ f_t \end{bmatrix} \equiv \begin{bmatrix} \frac{x_n}{r_n} & 0 & \frac{z_n}{r_n} \\ 0 & 1 & 0 \\ -\frac{z_n}{r_n} & 0 & \frac{x_n}{r_n} \end{bmatrix} \mathbf{f}_c$

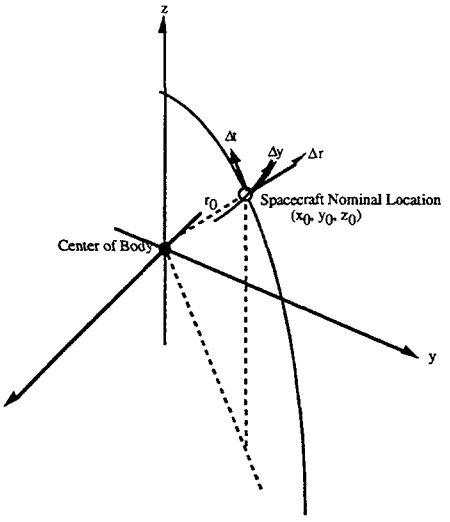

Figure 2: Coordinate around Nominal Hovering Point

With ideally tight altitude control using the gravity direction (f_r direction) thrusters, $\Delta r(t) \equiv 0$ will hold at all times, and Eq.12 will reduce to

$$\begin{bmatrix} \Delta \ddot{y} \\ \Delta \ddot{t} \end{bmatrix} - \frac{2\omega}{r_n} \begin{bmatrix} 0 & z_n \\ -z_n & 0 \end{bmatrix} \begin{bmatrix} \Delta \dot{y} \\ \Delta \dot{t} \end{bmatrix}$$

$$-\frac{\omega^2}{r_n^2} \begin{bmatrix} r_n^2 - \frac{1}{r_n} & 0 \\ 0 & z_n^2 - \frac{1}{r_n} \end{bmatrix} \begin{bmatrix} \Delta y \\ \Delta t \end{bmatrix} = \begin{bmatrix} f_y \\ f_t \end{bmatrix} \tag{13}$$

This equation describes linearized motion with tight control along the $\mathbf{r}_0$ direction. The stability of this controller can be investigated from the characteristic equation of Eq.13

$$s^4 + \omega^2 \left\{ \frac{2 - r_n^3}{r_n^3} + \frac{3z_n^2}{r_n^2} \right\} s^2$$

$$+\omega^4 \left(1 - \frac{1}{r_n^3}\right) \left(\frac{z_n^2}{r_n^2} - \frac{1}{r_n^3}\right) = 0 \tag{14}$$

The tightly controlled spacecraft motion is stable if and only if all roots of Eq.14 have negative or zero real parts. Note that Eq.14 corresponds to the zero locations of the open-loop spacecraft dynamics. So, the "tight" controller can be considered as the infinity limit of controller gain. Generally speaking, if the characteristic equation is

$$s^4 + bs^2 + c = 0 \tag{15}$$

then the stability conditions are

$$b \geq 0 \tag{16}$$

$$c \geq 0 \tag{17}$$

$$b^2 - 4c \geq 0 \tag{18}$$

In our case, these conditions become

$$\omega^2 \left\{ \frac{2 - r_n^3}{r_n^3} + \frac{3z_n^2}{r_n^2} \right\} \geq 0 \tag{19}$$

$$\omega^4 \left(1 - \frac{1}{r_n^3}\right) \left(\frac{z_n^2}{r_n^2} - \frac{1}{r_n^3}\right) \geq 0 \tag{20}$$

$$\omega^4 \left\{ \frac{2 - r_n^3}{r_n^3} + \frac{3z_n^2}{r_n^2} \right\}^2$$

$$-4\omega^4 \left(1 - \frac{1}{r_n^3}\right) \left(\frac{z_n^2}{r_n^2} - \frac{1}{r_n^3}\right) \geq 0 \tag{21}$$

or equivalently,

$$\left(\frac{z_n}{r_n}\right)^2 \geq \frac{-2 + r_n^3}{3r_n^3} \tag{22}$$

$$r_n \leq 1 \quad \text{or} \quad \left(\frac{z_n}{r_n}\right)^2 \geq \frac{1}{r_n^3} \tag{23}$$

$$\begin{cases} 1 \leq r_n \leq \sqrt[3]{4} & \text{or} \\ \left(\frac{z_n}{r_n}\right)^2 \geq \frac{5r_n^3 - 8 + \sqrt{(5r_n^3 - 8)^2 - 9r_n^6}}{9r_n^3} & \text{or} \\ \left(\frac{z_n}{r_n}\right)^2 \leq \frac{5r_n^3 - 8 - \sqrt{(5r_n^3 - 8)^2 - 9r_n^6}}{9r_n^3} \end{cases} \tag{24}$$

Eq.22, 23, and 24 corresponds to Eqs.19, 20, and 21, respectively. The hovering point is stable if and only if Eqs.22 – 24 holds at that point. Note that these equations hold if $r_n \leq 1$, because, at that time,

$$\frac{-2 + r_n^3}{3r_n^3} \leq 0$$

$$\frac{5r_n^3 - 8 + \sqrt{(5r_n^3 - 8)^2 - 9r_n^6}}{9r_n^3} \leq 0$$

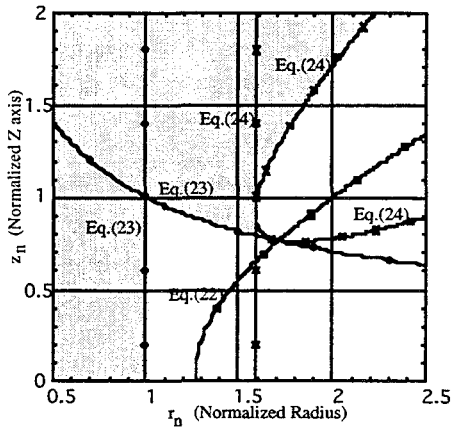

Figure 3: Stable Region for Tight Altitude Controlled Hovering over Point Mass — Shaded Region Corresponds to Stable Area

The stable area of the controller is summarized in Fig.3. It can be seen that the region of $r_n < 1$ i.e. the area within the resonance radius is stable.

Sufficient Conditions for Stable Hovering above an Arbitrary Body

The previous section derived the stable region for hovering over a point mass using a tight controller. This condition can be generalized to an arbitrary gravity field, but the resulting conditions do not lend themselves to analytical description. So, instead, a sufficient condition for the tight controller stability is discussed.

Starting from Eq.10, let the eigenvalues and eigenvectors of the matrix $\left[\frac{\partial^2 U}{\partial \mathbf{r}^2}\right]$ be α_1, α_2, α_3, and $\mathbf{v}_1$, $\mathbf{v}_2$, $\mathbf{v}_3$, respectively. As this matrix is symmetric, the eigenvectors are orthogonal to each other. So, without any loss of generality, we can define the following relations;

$$\mathbf{v}_1 \times \mathbf{v}_2 = \mathbf{v}_3 \quad (25)$$
$$\mathbf{v}_2 \times \mathbf{v}_3 = \mathbf{v}_1 \quad (26)$$
$$\mathbf{v}_3 \times \mathbf{v}_1 = \mathbf{v}_2 \quad (27)$$
$$\|\mathbf{v}_1\| = \|\mathbf{v}_2\| = \|\mathbf{v}_3\| = 1 \quad (28)$$

By changing our coordinates

$$\mathbf{x}' = [\mathbf{v}_1, \mathbf{v}_2, \mathbf{v}_3]^{-1} \begin{bmatrix} \Delta x \\ \Delta y \\ \Delta z \end{bmatrix} = \begin{bmatrix} \mathbf{v}_1^T \\ \mathbf{v}_2^T \\ \mathbf{v}_3^T \end{bmatrix} \begin{bmatrix} \Delta x \\ \Delta y \\ \Delta z \end{bmatrix} \quad (29)$$

Eq. 10 becomes

$$\begin{aligned} \ddot{\mathbf{x}}' &- 2\omega \begin{bmatrix} 0 & -v_{3z} & v_{2z} \\ v_{3z} & 0 & -v_{1z} \\ -v_{2z} & v_{1z} & 0 \end{bmatrix} \dot{\mathbf{x}}' \\ &- \left\{ \begin{bmatrix} \alpha_1+\omega^2 & 0 & 0 \\ 0 & \alpha_2+\omega^2 & 0 \\ 0 & 0 & \alpha_3+\omega^2 \end{bmatrix} \right. \\ &\left. - \omega^2 \begin{bmatrix} v_{1z} \\ v_{2z} \\ v_{3z} \end{bmatrix} [v_{1z}, v_{2z}, v_{3z}] \right\} \mathbf{x}' \\ &= \mathbf{f}' \end{aligned} \quad (30)$$

For most cases, one of the eigenvectors ($\mathbf{v}_3$, for example) is almost aligned with the gravity attraction, and 2 of the eigenvalues (α_1 , α_2) are stable, i.e. negative values. This is exactly true if the asteroid is a sphere. Here, $\mathbf{v}_3$ is defined as the "quasi-gravity"direction. By adopting the tight controller in the $\mathbf{v}_3$ direction (observation and thrusting), the system of Eq. 30 will reduce to

$$\begin{aligned} \ddot{\mathbf{x}}' &- 2\omega \begin{bmatrix} 0 & -v_{3z} \\ v_{3z} & 0 \end{bmatrix} \dot{\mathbf{x}}' \\ &- \left\{ \begin{bmatrix} \alpha_1+\omega^2 & 0 \\ 0 & \alpha_2+\omega^2 \end{bmatrix} \right. \\ &\left. -\omega^2 \begin{bmatrix} v_{1z} \\ v_{2z} \end{bmatrix} [v_{1z}, v_{2z}] \right\} \mathbf{x}' = \mathbf{f}' \end{aligned} \quad (31)$$

With characteristic equation

$$s^4 + bs^2 + c = 0 \quad (32)$$

where

$$b = 4\omega^2 v_{3z}^2 - k_1 - k_2 \quad (33)$$
$$c = -\omega^4 v_{1z}^2 v_{2z}^2 + k_1 k_2 \quad (34)$$
$$k_1 = \alpha_1 + \omega^2 - v_{1z}^2 \omega^2 \quad (35)$$
$$k_2 = \alpha_2 + \omega^2 - v_{2z}^2 \omega^2 \quad (36)$$

Now, the stability conditions of the tight controller are

$$b \geq 0 \quad (37)$$
$$c \geq 0 \quad (38)$$
$$b^2 - 4c \geq 0 \quad (39)$$

or,

$$3\omega^2 v_{3z}^2 + \omega^2 - (\alpha_1+\omega^2) - (\alpha_2+\omega^2) \geq 0 \quad (40)$$
$$(\alpha_1+\omega^2)(\alpha_2+\omega^2) - \omega^2 v_{1z}^2 (\alpha_2+\omega^2) - \omega^2 v_{2z}^2 (\alpha_1+\omega^2) \geq 0 \quad (41)$$
$$(\alpha_1 - \alpha_2 - \omega^2)^2 + 3\omega^4 v_{3z}^2 (v_{3z}^2 + 2) - 8\omega^2 v_{3z}^2 \{(\alpha_1+\omega^2) + (\alpha_2+\omega^2)\} \geq 0 \quad (42)$$

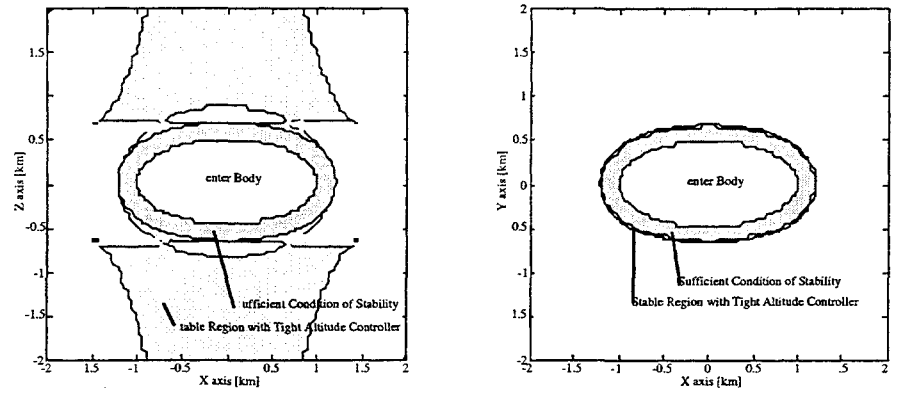

Figure 4: Stable Region for Tight Altitude Controlled Hovering over Ellipsoid with Rotation Period of 4.07[hour]

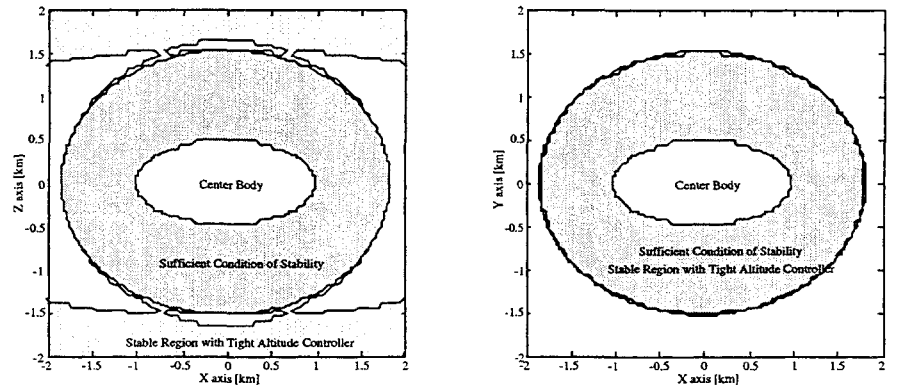

Figure 5: Stable Region for Tight Altitude Controlled Hovering over Ellipsoid with Rotation Period of 10.0[hour]

To obtain these equations, we should be aware of the following relations, which can be deduced from Eqs.25 – 28;

$$v_{1x}^2 + v_{2x}^2 + v_{3x}^2 = 1 \quad (43)$$
$$v_{1y}^2 + v_{2y}^2 + v_{3y}^2 = 1 \quad (44)$$
$$v_{1z}^2 + v_{2z}^2 + v_{3z}^2 = 1 \quad (45)$$
$$v_{1x}v_{1y} + v_{2x}v_{2y} + v_{3x}v_{3y} = 0 \quad (46)$$
$$v_{1x}v_{1z} + v_{2x}v_{2z} + v_{3x}v_{3z} = 0 \quad (47)$$
$$v_{1z}v_{1y} + v_{2z}v_{2y} + v_{3z}v_{3y} = 0 \quad (48)$$

Note that, without any loss of generality, we can assume

$$\alpha_1 \geq \alpha_2 \quad (49)$$

With Eq. 49, we see that Eq. 40 to 42 will hold if

$$\alpha_1 + \omega^2 \leq 0 \quad (50)$$
$$\alpha_2 + \omega^2 \leq 0 \quad (51)$$

Eqs.50 – 51 are the sufficient conditions for the "quasi-gravity" direction tight controller stability.

In the case of a sphere, we can assume that the spacecraft's nominal point is located on x-z plane, without any loss of generality. So, by assuming the spacecraft nominal position as (x, 0, z), the stability results reduce to

$$r \leq 1 \quad (52)$$

where $r = \sqrt{x^2 + z^2}$ and the length is normalized by $r_s \equiv \left(\frac{\mu}{\omega^2}\right)^{1/3}$

Numerical Check of Stable Area

To validate our sufficient condition, a number of numerical checks are conducted. Here, the center body is assumed to be an ellipsoid (Figs.4 – 5), or the realistic shape of asteroid Castalia (Hudson and Ostro 1994) (Figs.6 – 7). The rotation period is

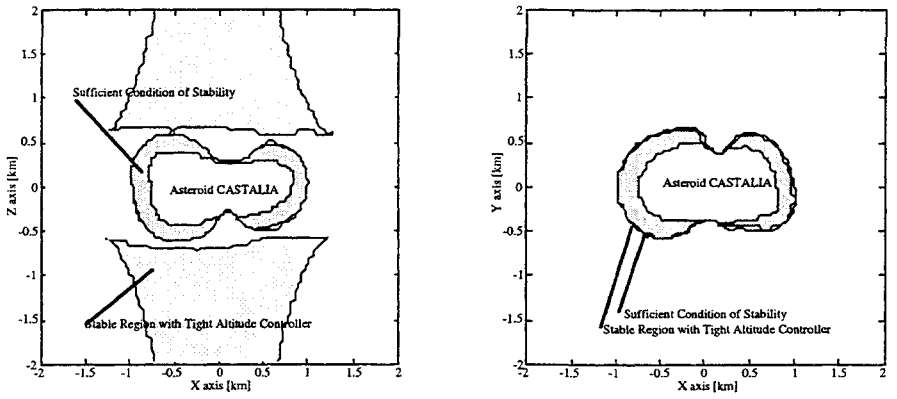

Figure 6: Stable Region for Tight Altitude Controlled Hovering over Castalia with Rotation Period of 4.07[hour]

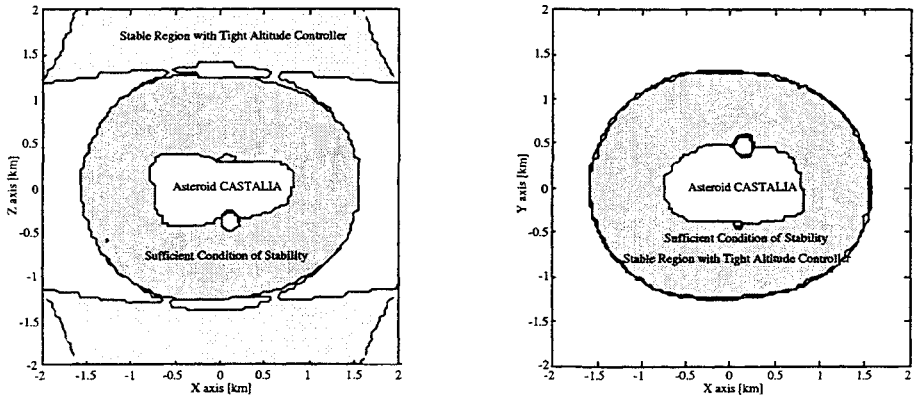

Figure 7: Stable Region for Tight Altitude Controlled Hovering over Castalia with Rotation Period of 10.0[hour]

taken as 4.07 hours, which is Castalia's estimated rotation period, or 10 hours, for comparison. From Figs.3 – 7, it seems that the stable region has some similarity among the sphere, ellipsoid and Castalia center body cases, still, the similarity degrades at the faster rotation speed. Figs.4 – 7 also show the sufficient condition area derived from the discussion of the previous section. It can be seen that the sufficient areas coincide well with the actual stable area, if the region of interest is near the asteroid surface.

Fig.8 shows the fastest and slowest residual mode of a tightly controlled spacecraft. Even if the hovering is stable, the frequencies of the residual modes are a matter of interest. If they are too fast, the hovering trajectory can become unstable easily with a small time lag in the controller. In contrary, if the residual mode is too slow, the hovering position deviation can become excessively large with only small initial velocity errors. These figures imply that hovering near the stability limit does not have strong robustness against velocity errors.

Summary

In this section, the stability of hovering under tight control has been discussed. The stability conditions are deduced explicitly for the point mass, and we find that hovering is stable for the region inside the resonance radius. For a general mass distribution analytical results are not possible, so reliance must be made on numerical checks of stability. We are able to derive a simpler sufficient condition in this case which agrees well with the full stability conditions.

Also from this stability analysis, it is clear that hovering using the controller proposed here should be most robust near the center body regions. The maximum altitude for the stable hovering can be defined as the resonance radius, or the radius at which Eqs.50 – 51 hold.

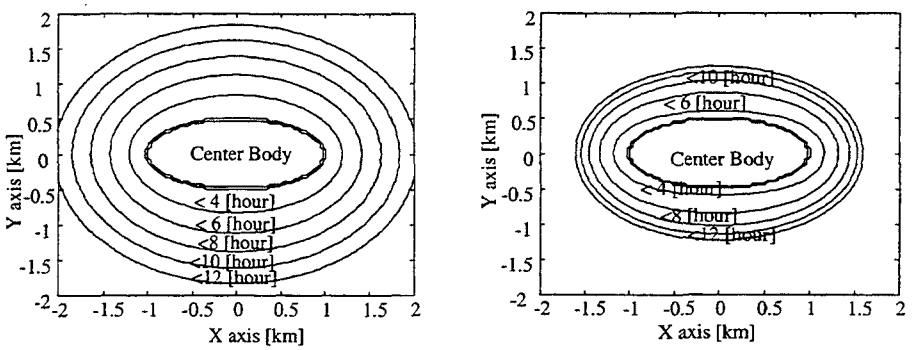

Figure 8: Maximum and Minimum Residual Mode Frequency of Tight Controller Around the Ellipsoidal Body with 10 hour Rotation

Sensitivity to Control Direction Error

For an actual spacecraft, some discrepancy will exist among the thrust that cancels the centrifugal force, the estimated direction of gravity attraction, and the hovering altitude. Ideally, the hovering equilibrium point will be the point where these coincide with their prescribed values. But actually, there will be some inconsistency among them, and there will be no points where they coincide exactly with the prescribed values. The actual equilibrium point will be a compromise among these values.

In this section, our discussions will be made using the linearized equations for simplicity. The linearized equation of motion for hovering is

$$\ddot{\mathbf{x}} - 2\omega \begin{bmatrix} 0 & -1 & 0 \\ 1 & 0 & 0 \\ 0 & 0 & 0 \end{bmatrix} \dot{\mathbf{x}} - \left\{ \begin{bmatrix} \omega^2 & 0 & 0 \\ 0 & \omega^2 & 0 \\ 0 & 0 & 0 \end{bmatrix} + \left[\frac{\partial^2 U}{\partial \mathbf{r}^2}\right] \right\} \mathbf{x} = \mathbf{f}_c \quad (53)$$

$$\mathbf{f}_c = \mathbf{f}_{c,g} + \mathbf{f}_{c,c} \quad (54)$$

where $\mathbf{x}$ is the deviation of the spacecraft from the nominal point, $\mathbf{f}_{c,g}$ is the control force of gravity direction, and $\mathbf{f}_{c,c}$ is the force to cancel the centrifugal force, which is added in an open-loop manner. The nominal position $\mathbf{x} = 0$ is defined as a position where the gravity attraction is aligned with the control force $\mathbf{f}_{c,g}$, and where the hovering altitude becomes the prescribed value.

Here, we assume that $\mathbf{f}_{c,c}$ is the force which is balanced with the actual centrifugal force at the position $\mathbf{x}_c$. Ideally, $\mathbf{x}_c = 0$ holds. But due to errors, including the gravity direction estimation error, $\mathbf{x}_c$ will not coincide with the nominal position of $\mathbf{x} = 0$.

In this case, Eq.53 will be as

$$\ddot{\mathbf{x}} - 2\omega \begin{bmatrix} 0 & -1 & 0 \\ 1 & 0 & 0 \\ 0 & 0 & 0 \end{bmatrix} \dot{\mathbf{x}} - \left\{ \begin{bmatrix} \omega^2 & 0 & 0 \\ 0 & \omega^2 & 0 \\ 0 & 0 & 0 \end{bmatrix} + \left[\frac{\partial^2 U}{\partial \mathbf{r}^2}\right] \right\} \mathbf{x} = \mathbf{f}_{c,g} + \begin{bmatrix} \omega^2 & 0 & 0 \\ 0 & \omega^2 & 0 \\ 0 & 0 & 0 \end{bmatrix} \mathbf{x}_c \quad (55)$$

At the equilibrium point, $\ddot{\mathbf{x}}$ and $\dot{\mathbf{x}}$ is equal to zero, so

$$\left[\frac{\partial^2 U}{\partial \mathbf{r}^2}\right] \mathbf{x} + \begin{bmatrix} \omega^2 & 0 & 0 \\ 0 & \omega^2 & 0 \\ 0 & 0 & 0 \end{bmatrix} (\mathbf{x} - \mathbf{x}_c) = \mathbf{f}_{c,g} \quad (56)$$

or

$$A\mathbf{x} = B\mathbf{x}_c + f\mathbf{v}_g \quad (57)$$

where

$$A \equiv \left[\frac{\partial^2 U}{\partial \mathbf{r}^2}\right] + \begin{bmatrix} \omega^2 & 0 & 0 \\ 0 & \omega^2 & 0 \\ 0 & 0 & 0 \end{bmatrix} \quad (58)$$

$$B \equiv \begin{bmatrix} \omega^2 & 0 & 0 \\ 0 & \omega^2 & 0 \\ 0 & 0 & 0 \end{bmatrix} \quad (59)$$

$$\mathbf{f}_{c,g} \equiv f\mathbf{v}_g \quad (60)$$

$$\|\mathbf{v}_g\| = 1 \quad (61)$$

$$\|\mathbf{f}_{c,g}\| = f \quad (62)$$

holds. Note that the direction of $\mathbf{f}_{c,g}$ aligns with the estimated gravitational attraction, which acts to keep the altitude along the $\mathbf{f}_{c,g}$ direction equal to a constant height. At the equilibrium point, this control force must be constant.

Suppose matrix A is not singular, then Eq.57 can be rewritten as

$$\mathbf{x} = A^{-1}B\mathbf{x}_c + fA^{-1}\mathbf{v}_g \quad (63)$$

and

$$\mathbf{v}_g^T\mathbf{x} \equiv r_0 = \mathbf{v}_g^T A^{-1} B\mathbf{x}_c + f\mathbf{v}_g^T A^{-1}\mathbf{v}_g \quad (64)$$

$$f = \frac{r_0}{\mathbf{v}_g^T A^{-1}\mathbf{v}_g} - \frac{1}{\mathbf{v}_g^T A^{-1}\mathbf{v}_g}\mathbf{v}_g^T A^{-1} B\mathbf{x}_c \quad (65)$$

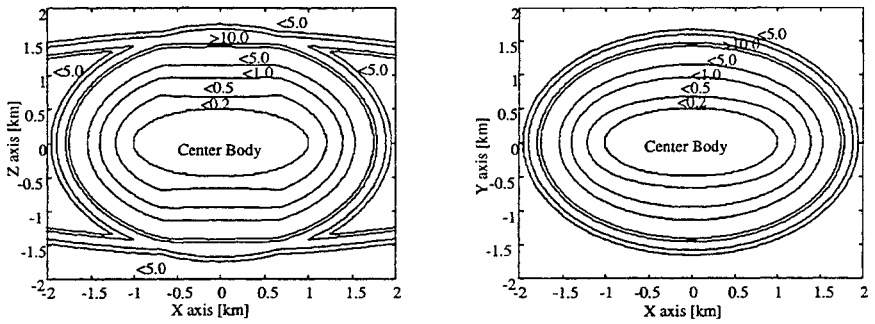

Figure 9: Sensitivity of Equilibrium Point Due to Gravity Direction Estimation Error

where r_0 is the difference of altitude between the linearized center ($\mathbf{x} = \mathbf{0}$) and the commanded altitude, and r_0 $(= \mathbf{v}_g^T \mathbf{x})$ $= 0$ holds from the definition of $\mathbf{x}$. The control force $\mathbf{f}_{c,g}$ will keep the altitude as commanded, meaning that $\mathbf{v}_g \cdot \mathbf{x} = r_0$ will hold. From Eq.63,

$$\mathbf{v}^T \mathbf{x} = \mathbf{v}^T A^{-1} B \mathbf{x}_c + f \mathbf{v}^T A^{-1} \mathbf{v}_g \quad (66)$$

holds for arbitrary vector $\mathbf{v}$. From Eqs.65 and 66, we get

$$\mathbf{v}^T \mathbf{x} = \mathbf{v}^T A^{-1} B \mathbf{x}_c + f \mathbf{v}^T A^{-1} \mathbf{v}_g \quad (67)$$

$$= \mathbf{v}^T \left\{ I - \frac{A^{-1} \mathbf{v}_g \mathbf{v}_g^T}{\mathbf{v}_g^T A^{-1} \mathbf{v}_g} \right\} A^{-1} B \mathbf{x}_c \quad (68)$$

As this equation holds for arbitrary vector $\mathbf{v}$,

$$\mathbf{x} = \left\{ I - \frac{A^{-1} \mathbf{v}_g \mathbf{v}_g^T}{\mathbf{v}_g^T A^{-1} \mathbf{v}_g} \right\} A^{-1} B \mathbf{x}_c \quad (69)$$

This equation relates the sensitivity of equilibrium point ($\mathbf{x}$) with $\mathbf{x}_c$ (the discrepancy between the centrifugal force reference point and the gravity direction reference point). So, by defining

$$M \equiv \left\{ I - \frac{A^{-1} \mathbf{v}_g \mathbf{v}_g^T}{\mathbf{v}_g^T A^{-1} \mathbf{v}_g} \right\} A^{-1} B \quad (70)$$

the maximum singular value of matrix M must be kept small to have equilibrium points insensitive to these errors.

The eigenvectors of matrix M have some interesting characteristics. For example, as

$$\mathbf{v}_g^T M = \left\{ \mathbf{v}_g^T - \frac{\mathbf{v}_g^T A^{-1} \mathbf{v}_g \mathbf{v}_g^T}{\mathbf{v}_g^T A^{-1} \mathbf{v}_g} \right\} A^{-1} B = \mathbf{0} \quad (71)$$

the eigenvectors of non-zero eigenvalues must be perpendicular to the vector $\mathbf{v}_g$. And,

$$B \begin{bmatrix} 0 \\ 0 \\ 1 \end{bmatrix} = \mathbf{0} \quad (72)$$

means that the z axis (= spin axis) direction is one of the eigenvectors with an eigenvalue of zero.

Fig.9 is the numerical calculation of the maximum singular value of matrix M. Note that the equilibrium point becomes insensitive to errors as the hovering point approaches closer to the asteroid.

Numerical examples

Some numerical simulations of hovering trajectories were conducted. The controller adopted here performs as a tight controller along the estimated gravity direction. Centrifugal force cancellations are added periodically, the added force to cancel it is only the component perpendicular to the gravity force direction. The residual component which aligns with the gravity direction is applied through the closed loop tight control.

The tight controller is of dead band type. If the range to the center body along the estimated gravity direction exceeds the prescribed value, the thruster will be fired. The estimated gravity direction is kept unchanged within each simulation. The control logic which checks if the spacecraft violates the dead band is activated every 1 sec.

Additionally, no open-loop logic to cancel the nominal gravity attraction is used as the quasi-continuous force to kill out the gravity force can be obtained through the closed-loop control.

Simulations were executed to evaluate the robustness of hovering associated with the hovering position. For most cases, the center body is assumed to be the ellipsoid of dimensions $0.5[km] \times 0.5[km] \times 1.0[km]$. Two hovering positions were selected to show the difference between hovering near the center body at (0.65km, 0.00km, 0.50km) and further at (1.65km, 0.00km, 0.50km),just as shown in Fig.10. Some other simulations were made to evaluate hovering in the unstable region and hovering over Castalia. In this section, the rotation period of the center body is assumed to be 10 hours.

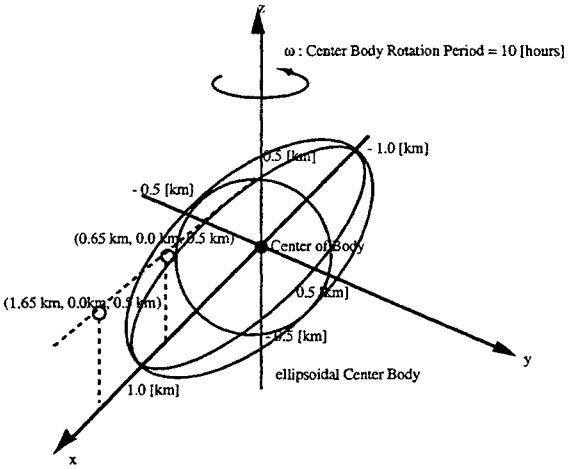

Figure 10: Hovering Positions at Numerical Simulations

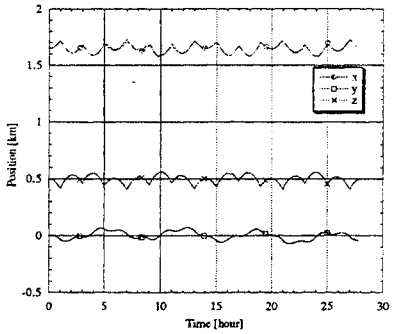

Figure 11: Hovering Simulation Over Ellipsoid with Centrifugal Cancel Period of 2.0 [hour]: hovering at region near the resonance radius

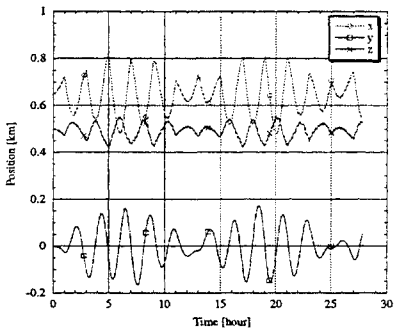

Figure 12: Hovering Simulation Over Ellipsoid with Centrifugal Cancel Period of 2.0 [hour]: hovering at region close to the center body

Simulations on Centrifugal Force Cancel Period Effect

In (Scheeres 1999), continuous acceleration was assumed to cancel the centrifugal force. But in reality, the most popular thrusting device for spacecraft are chemical thrusters, which produce impulsive accelerations. By adjusting the duration of firing and the period of the cycle, a spacecraft can simulate continuous thrusting. In this case, by using an improperly long cycle period, the spacecraft may fail to hover above the small body even if the prescribed position is in the stable region.

Fig.11 – 12 show the hovering simulation with the centrifugal cancel cycle period of 2.0 hours. Each figure shows the time history along the x, y, and z axis. If hovering is stable and steady, the lines will be straight. Here, the dead band width of the range is assumed to be ±1 cm. No initial errors and no navigation errors are assumed.

It is true that the acceptable period depends somewhat on the position of hovering. Still by noting that the rotating period of center body is 10 hours in these cases, it is clear that the centrifugal force cancel period is not very sensitive to the hovering stability.

Simulations on Range Allowance Effect

Fig.13 – 14 show the hovering simulations with a range deadband width of 100 [m]. Each figure shows the time history along the x, y, and z axis. Here, centrifugal force cancellation thrusts are assumed to be fired every 0.1 hour. No initial errors and no navigation errors are assumed. The delta-V for tight hovering control is 2.0 cm/sec.

It is clear that the range allowance is not sensitive to the hovering stability. Still it should be noted that the delta-V magnitude to maintain the range should be adjusted carefully to properly cancel the spacecraft velocity. If their values are excessively small, the spacecraft can not produce the necessary acceleration to cancel the gravity force. In contrast, if they are too large, it results in a limit cycle of very short period.

Simulations of Velocity Error Effect

The initial velocity of the spacecraft is one of the factors that decide the amplitude of the hovering position oscillation. If the frequency of the residual motion mode is low, the amplitude will be sensitive to the initial velocity error. Fig. 15 – 16 show the

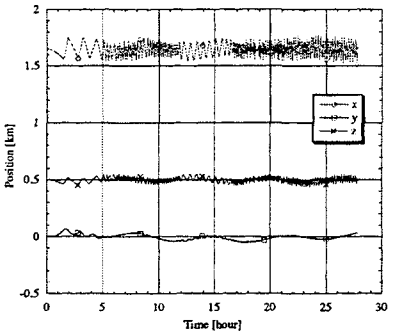

Figure 13: Hovering Simulation Over Ellipsoid with Dead Band Width of 100 [m]: hovering at region near the resonance radius

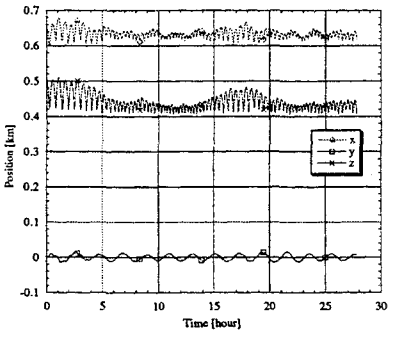

Figure 14: Hovering Simulation Over Ellipsoid with Dead Band Width of 100 [m]: hovering at region close to the center body

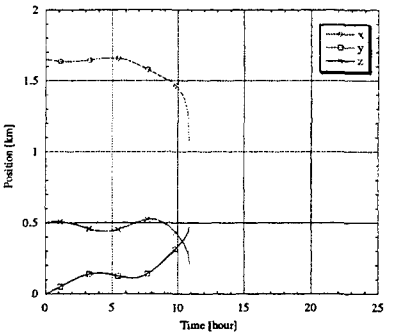

Figure 15: Hovering Simulation Over Ellipsoid with Initial Velocity Error of 1.0[cm/sec]: hovering at region near the resonance radius

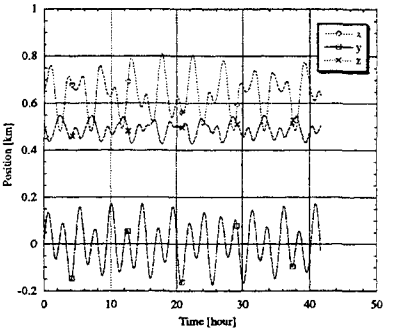

Figure 16: Hovering Simulation Over Ellipsoid with Initial Velocity Error of 10.0[cm/sec]: hovering at region close to the center body

simulations with initial velocity errors. Here, the range allowance is assumed to be 1cm, and centrifugal force is canceled every 0.1 hour. No guidance errors and no initial position errors are assumed.

It is shown that the acceptable velocity error depends strongly on the position of hovering. If the hovering position is near the resonance radius and has slow residual modes, it is sensitive to the initial velocity. But if the hovering position is close to the center body, relatively large initial velocity errors (comparable to escape velocity) can be accommodated.

Simulations on Gravity Estimation Error Effect

At the actual hovering position, the estimated gravity attraction and centrifugal forces are not consistent, and the actual settling point is affected by this mismatch. If the estimated gravity attraction is not of the prescribed position but is displaced by $(\Delta x, \Delta y, \Delta z)$ from that position, the hovering is disturbed. Fig.17 – 18 show this effect. Here, the range allowance is assumed to be 1cm, and centrifugal force is canceled every 0.1 hour. No guidance errors and no initial errors are assumed. The delta-V amount is set as a function of the spacecraft velocity along the estimated gravity direction.

It is shown that hovering is sensitive to these errors if the commanded hovering point is near the resonance radius. Fig.18 suggests that hovering close to the center body is robust against gravity estimation error.

Some Other Simulations

Fig.19 shows a hovering simulation in the unstable region. It can be seen that the hovering trajectory goes away with very small initial velocity error. Fig.20 shows hovering over Castalia with a rotation period of 10 hours.

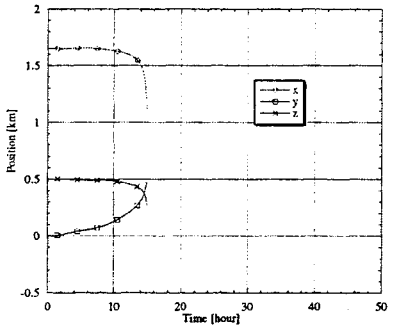

Figure 17: Hovering Simulation Over Ellipsoid with Gravity Direction Discrepancy of 10[m]: hovering at region near the resonance radius

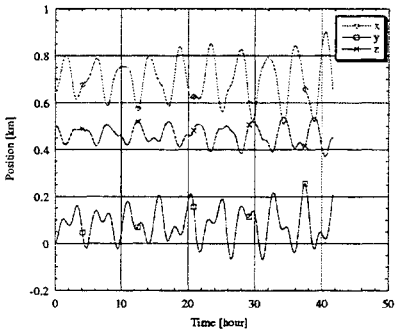

Figure 18: Hovering Simulation Over Ellipsoid with Gravity Direction Discrepancy of 100[m]: hovering at region close to the center body

Note that in this section, we do not investigate the influence of rotation period estimation error. It is expected that it will be estimated well in advance of hovering.

Conclusion

This paper discuss hovering over a uniformly rotating small asteroid. It is assumed that the spacecraft is equipped with an altimeter, and the controller commands thrusting to keep the altimeter output constant. It is found that the hovering is stable within a region nearer than the resonance radius for the point mass central body case, and at the equivalent near central body region for the arbitrary central body case. It is also found that the robustness of the hovering trajectory to controller error increases as the hovering position becomes closer to the center body.

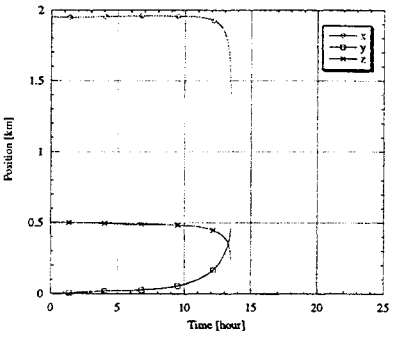

Figure 19: Hovering Simulation Over Ellipsoid around the Unstable Point of [1.95km, 0.0km, 0.5km]

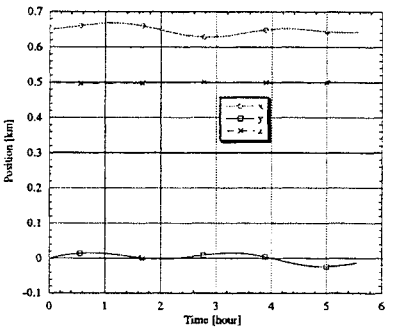

Figure 20: Hovering Simulation Over Castalia

Acknowledgements

The work described here was funded in part by the TMOD Technology Program by a grant from the Jet Propulsion Laboratory, California Institute of Technology which is under contract with the National Aeronautics and Space Administration. Support for S. Sawai was from a Fellowship from the Ministry of Education, Japan.

References

1) Hudson, R.S., S.J. Ostro. "Shape of Asteroid 4769 Castalia (1989 PB) from inversion of radar images". *Science* 263, 940–943, 1994.

2) Scheeres, D.J. "Stability of Hovering Orbits around Small Bodies". AAS Paper 99-159,1999 AAS/AIAA Spaceflight Mechanics Meeting, February 1999.

3) Scheeres, D.J., B.G. Williams, J.K. Miller. "Evaluation of the Dynamic Environment of an Asteroid: Applications to 433 Eros". Journal of Guidance, Control, and Dynamics 23: 466–475, 2000